

The Transit Light Curve Project.

IX. Evidence for a Smaller Radius of the Exoplanet XO-3b

Joshua N. Winn¹, Matthew J. Holman², Guillermo Torres², Peter McCullough³, Christopher Johns-Krull⁴, David W. Latham², Avi Shporer⁵, Tsevi Mazeh⁵, Enrique Garcia-Melendo⁶, Cindy Foote⁷, Gil Esquerdo², Mark Everett⁸

ABSTRACT

We present photometry of 13 transits of XO-3b, a massive transiting planet on an eccentric orbit. Previous data led to two inconsistent estimates of the planetary radius. Our data strongly favor the smaller radius, with increased precision: $R_p = 1.217 \pm 0.073 R_{\text{Jup}}$. A conflict remains between the mean stellar density determined from the light curve, and the stellar surface gravity determined from the shapes of spectral lines. We argue the light curve should take precedence, and revise the system parameters accordingly. The planetary radius is about 1σ larger than the theoretical radius for a hydrogen-helium planet of the given mass and insolation. To help in planning future observations, we provide refined transit and occultation ephemerides.

Subject headings: planetary systems — stars: individual (XO-3, GSC 03727–01064)

¹Department of Physics, and Kavli Institute for Astrophysics and Space Research, Massachusetts Institute of Technology, Cambridge, MA 02139, USA

²Harvard-Smithsonian Center for Astrophysics, 60 Garden Street, Cambridge, MA 02138, USA

³Space Telescope Science Institute, 3700 San Martin Dr., Baltimore, MD 21218

⁴Dept. of Physics and Astronomy, Rice University, 6100 Main Street, MS-108, Houston, TX 77005

⁵Wise Observatory, Raymond and Beverly Sackler Faculty of Exact Sciences, Tel Aviv University, Tel Aviv 69978, Israel

⁶Esteve Duran Observatory, El Montanya, 08553 Seva, Barcelona, Spain

⁷Vermillion Cliffs Observatory, 4175 E. Red Cliffs Drive, Kanab, Utah, 84741

⁸Planetary Science Institute, 1700 E. Fort Lowell Rd., Suite 106, Tucson, AZ 85719

1. Introduction

The most intimate details about exoplanets have come from observations of transits and occultations, as recently reviewed by Charbonneau et al. (2007a), Ksanfomality (2007), and Seager (2008). This is the ninth publication of the Transit Light Curve (TLC) project, a series of photometric investigations of transiting exoplanets. The short-term goal of this project is the accurate determination of planetary radii and other system parameters (Holman et al. 2007, Winn et al. 2007a), the intermediate-term goal is detecting reflected light or thermal emission with ground-based observations (Winn et al. 2008), and the longer-term goal is seeking evidence for additional planets or satellites in the pattern of measured transit times (Holman & Murray 2005, Agol et al. 2005).

This paper is concerned with the determination of system parameters for XO-3, which was discovered by Johns-Krull et al. (2008; hereafter, JK), as part of the XO Project (McCullough et al. 2005). In this system, a planet with a mass near the deuterium-burning limit of $13 M_{\text{Jup}}$ orbits an F5V star, with a period of 3.19 d and an eccentricity of 0.26. The planet is the most massive transiting planet yet reported. It is also one of only 4 transiting planets with an obviously noncircular orbit. How such a massive planet formed, how it achieved its tight orbit, and why the orbit is eccentric, are interesting unanswered questions, and precise determinations of the basic system parameters may help to answer them.

JK found that a key parameter—the planetary radius—was especially uncertain, with an allowed range from 1.17 to 2.10 times the radius of Jupiter. This wide range encompassed the results of two different methods for determining the planetary radius that gave discrepant values. They found that if the true radius is near the low end of this range, it can be accommodated by ordinary models for gas giants of solar composition with the given mass and degree of insolation, while if the radius is near the high end of the allowed range, more complex and interesting models would require consideration (see, e.g., Guillot & Showman 2002, Bodenheimer et al. 2003, Chabrier & Baraffe 2007, Hansen & Barman 2007, Burrows et al. 2007).

High-precision photometry of transits is one avenue for improving the precision of the radius measurement. In § 2, we describe our observations and the production of the light curves. In § 3, we describe the procedure with which we estimated the system parameters from the light curves. In § 4, we present the results for the planetary, stellar, and orbital parameters, as well as the transit times and updated transit and occultation ephemerides, which are useful for planning future observations. In § 5 we summarize, and revisit the issue of the planetary radius and its theoretical interpretation, in light of the new data.

2. Observations and Data Reduction

We observed XO-3 on 12 nights when transits were predicted to occur according to the ephemeris of JK. The observing dates and other pertinent characteristics of the observations are given in Table 1.

On six of those nights, we used the 1.2m telescope at the Fred L. Whipple Observatory (FLWO) on Mt. Hopkins, Arizona. We used KeplerCam (Szentgyorgi et al. 2005), which has a monolithic 4096^2 CCD detector giving a $23'1 \times 23'1$ field of view. We binned the images 2×2 , giving a scale of $0''.68$ per binned pixel. We used a Sloan z filter, the reddest broad band filter available, to minimize the effects of stellar limb darkening on the transit light curves. On each night we attempted to observe as much of the transit as possible, preferably starting at least 1 hr prior to ingress and ending at least 1 hr after egress, although this was not always possible. We defocused the telescope slightly to permit exposure times of 10-15 s without saturating the brightest star in the field. We also obtained dome-flat exposures and bias exposures for calibration purposes.

On the other 6 nights, data were obtained with smaller telescopes. On the night of 2008 Feb 10, we used the 0.5m telescope at Wise Observatory, in Israel. We used a Santa Barbara Instrument Group (SBIG) ST-10 XME CCD detector with 2148×1472 pixels, giving a field of view of $40'5 \times 27'3$ and a scale of $1''.1$ per pixel. No filter was used. More details about this telescope and instrument are given by Brosch et al. (2008). On 2007 Oct 9, we used two different telescopes at Vermillion Cliffs Observatory, in Kanab, Utah: a 0.4m telescope with an SBIG ST-7e CCD (1530×1020 pixels, $0''.87$ pixel $^{-1}$, $22'2 \times 14'8$ FOV), and a 0.6m telescope with an SBIG ST-8xe CCD (765×510 pixels, $1''.31$ pixel $^{-1}$, $16'8 \times 11'2$ FOV). We used an I -band filter on the 0.4m telescope and an R -band filter on the 0.6m telescope. Each telescope was used to produce an independent light curve. On 2007 Sep 16, Oct 18, Oct 21, and Nov 6, we used a 0.6m telescope with an SBIG ST-9XE CCD, located at Esteve Duran Observatory in Seva, Spain. An I -band filter was used for the first three of these events, and a V -band filter was used for the Nov 06 event.

We used standard procedures for the overscan correction, trimming, bias subtraction, and flat-field division. For the FLWO and Wise data, we performed aperture photometry of XO-3 and 15-20 comparison stars. The flux of XO-3 was divided by the sum of the fluxes of the comparison stars, and then divided by a constant to give a unit mean flux outside of transit. For the other data, only 2 comparison stars were used. It was found in almost all cases that the out-of-transit (OOT) flux was not a constant over the course of the night, perhaps due to the effects of differential atmospheric extinction or slow drifts in focus, pixel position, or other external variables. To compensate, we solved for the “OOT baseline function,” a linear function of time, as part of the fitting process described in the

next section. Figures 1 and 2 show the final light curves. Figure 3 is a composite z -band light curve based on all of the FLWO data. Table 2 provides all of the data in numerical form.

3. Determination of System Parameters

In order to determine the stellar, planetary, and orbital parameters, we fitted a parametric model to the 13 photometric time series, as well as the 21 radial velocity measurements of JK. Our model and fitting method were similar to those described in previous TLC papers (see, e.g., Holman et al. 2006, Winn et al. 2007a). It is based on a Keplerian orbit of two spherical bodies. The physical parameters were the stellar mass and radius (M_\star and R_\star); the planetary mass and radius (M_p , R_p); the orbital period, inclination, eccentricity, and argument of pericenter (P , i , e , ω); and a particular midtransit time (T_c). In addition, for each of the two velocity data sets presented by JK (from the Hobby-Eberly Telescope and the Harlan J. Smith telescope), we allowed for an arbitrary additive constant velocity. As mentioned in the previous section, we also fitted for a linear function of time describing the OOT flux (2 parameters per light curve).

A well-known degeneracy involves both of the bodies’ masses and radii. Only 3 of those 4 parameters can be determined independently. Three parameters that *can* be determined independently are R_p/R_\star , M_\star/R_\star^3 (Seager & Mallen-Ornelas 2003), and M_p/R_p^2 (Southworth et al. 2007). Rather than reparameterizing in terms of those variables, we find it more convenient to fix the stellar mass at some fiducial value and then use the scaling relations $R_\star \propto M_\star^{1/3}$, $R_p \propto M_\star^{1/3}$, and $M_p \propto M_\star^{2/3}$ as needed.

To calculate the relative flux as a function of the projected separation of the planet and the star, we employed the analytic formulas of Mandel & Agol (2002) to compute the integral of the intensity over the unobscured portion of the stellar disk. We assumed the limb darkening law to be quadratic. In some previous studies, including our own, the limb-darkening coefficients have been fixed at the tabulated values based on stellar-atmosphere models. A more conservative approach is to fit for the limb-darkening law, since the actual stellar brightness distribution is not known and may differ from the tabulated limb-darkening law. However, it is generally not possible to constrain more than one free parameter in the limb-darkening law. Following the suggestion by Southworth (2008), our approach was to allow the linear coefficient (a) to vary freely, and to fix the quadratic coefficient (b) at the appropriate value tabulated by Claret (2004). To determine the “theoretical” values of the limb-darkening coefficients, we interpolated the ATLAS tables for the stellar parameters $T_{\text{eff}} = 6429$ K, $\log g = 4.244$ (cgs), $[\text{Fe}/\text{H}] = -0.177$ and $v_t = 2.0$ km s $^{-1}$. The interpolated

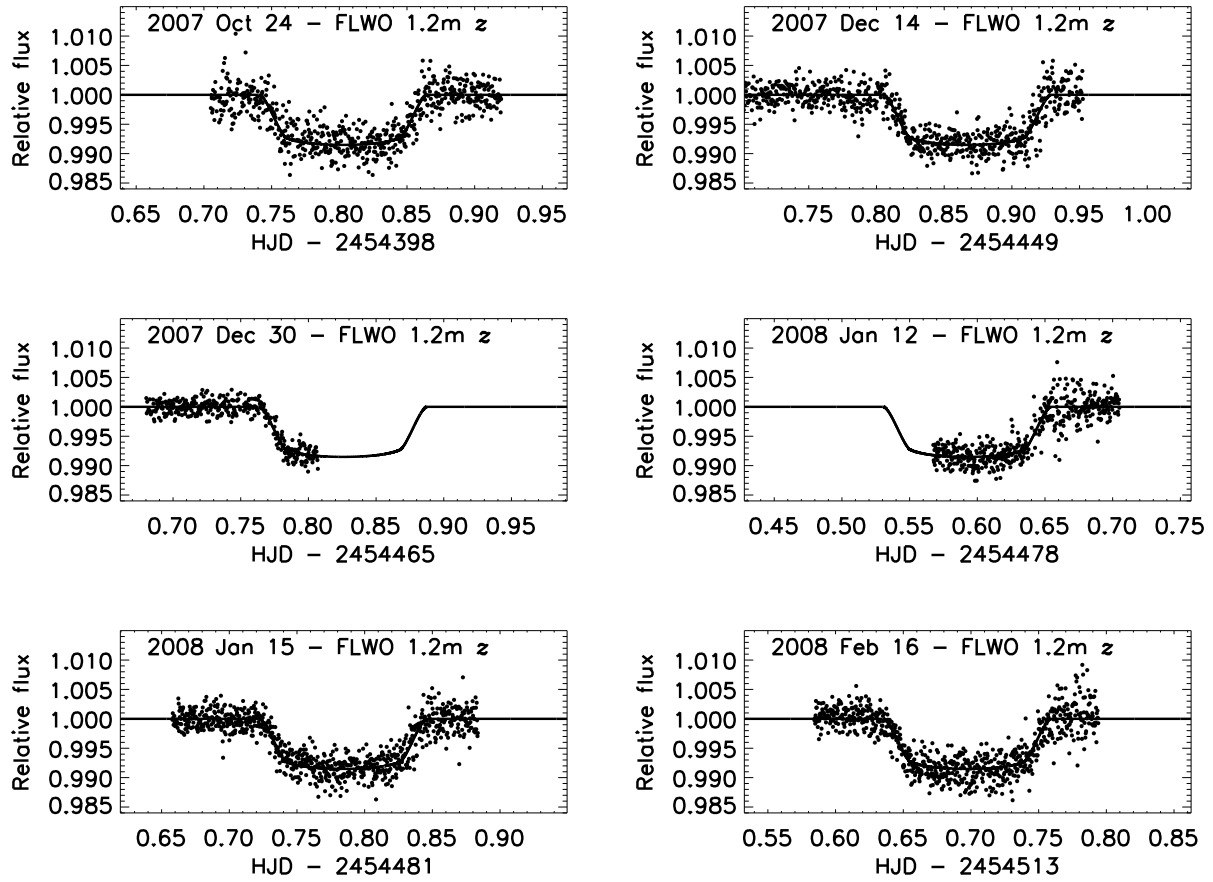


Fig. 1.— Relative z -band photometry of XO-3, based on observations with the FLWO 1.2m telescope.

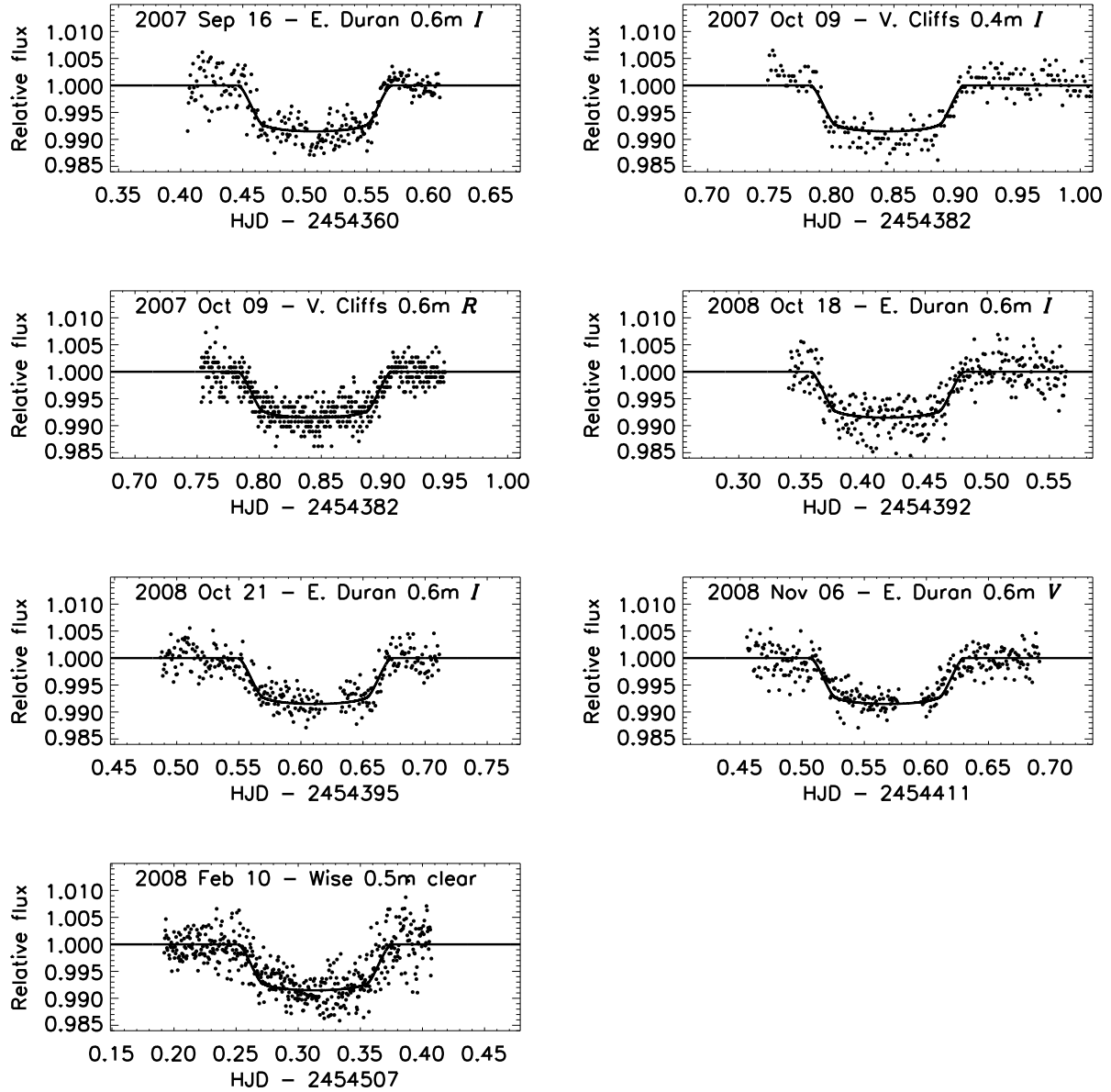


Fig. 2.— Relative photometry of XO-3, based on observations with 0.4–0.6m telescopes.

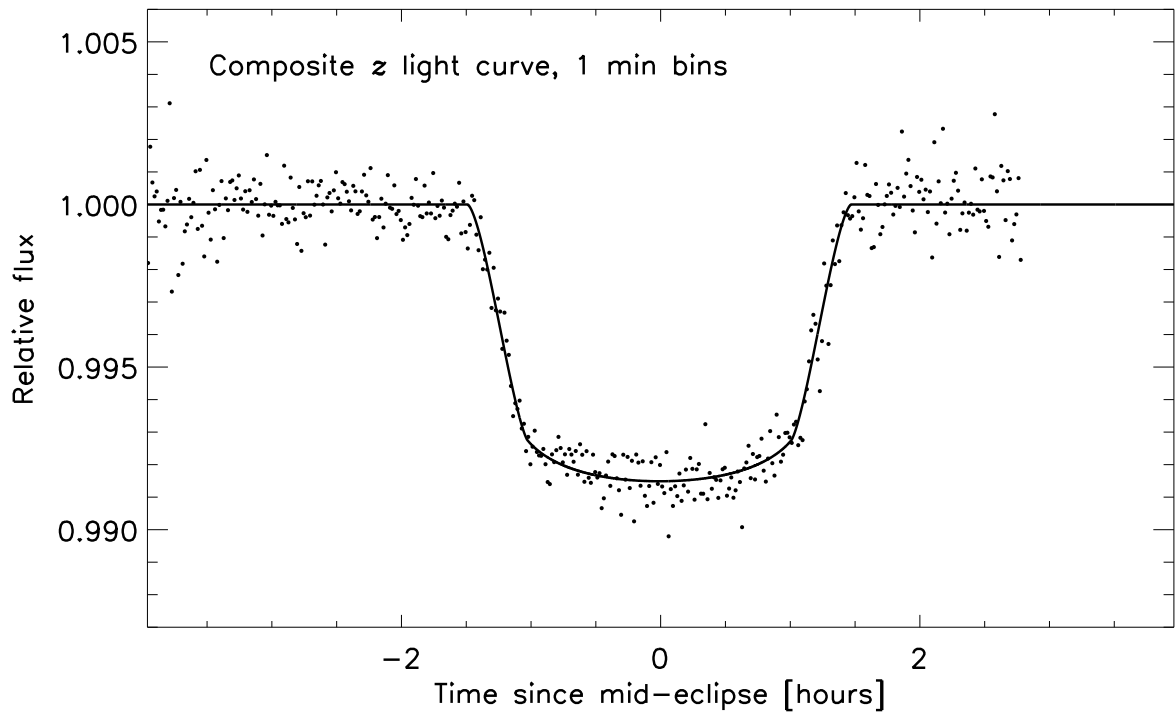


Fig. 3.— Composite z -band light curve of XO-3, calculated by subtracting the midtransit time from each time stamp, and then averaging into 1 min bins.

values are given in Table 4, as well as the results for the fitted linear coefficient.

The fitting statistic was

$$\chi^2 = \sum_{j=1}^{21} \left[\frac{v_j(\text{obs}) - v_j(\text{calc})}{\sigma_{v,j}} \right]^2 + \sum_{j=1}^{6104} \left[\frac{f_j(\text{obs}) - f_j(\text{calc})}{\sigma_{f,j}} \right]^2, \quad (1)$$

where $v_j(\text{obs})$ is the radial velocity observed at time j , $\sigma_{v,j}$ is the corresponding uncertainty, and $v_j(\text{calc})$ is the calculated radial velocity. A similar notation applies to the fluxes f . For the velocity uncertainties, we used the values reported by JK. For the flux uncertainties, we used a procedure that attempts to account for time-correlated (“red”) noise, at least approximately. For each of the 13 observed transits, we set the uncertainty of each data point equal to the root-mean-squared (rms) relative flux observed out of transit, multiplied by a factor $\beta \geq 1$. The factor β was determined using two different methods (described at the end of this section), and the larger of the two results was used in our final analysis.

We found the “best fitting” values of the model parameters, and their uncertainties, using a Markov Chain Monte Carlo (MCMC) algorithm [see Tegmark et al. (2004) for applications to cosmological data, Ford (2005) for radial-velocity data, Holman et al. (2006) or Winn et al. (2007) for our particular implementation, and Burke et al. (2007) for a similar approach]. This algorithm creates a chain of points in parameter space by iterating a jump function, which in our case was the addition of a Gaussian random deviate to a randomly-selected single parameter. If the new point has a lower χ^2 than the previous point, the jump is executed; if not, the jump is executed with probability $\exp(-\Delta\chi^2/2)$. We set the sizes of the random deviates such that $\sim 40\%$ of jumps are executed. We create a number of chains from different starting conditions to verify they all converge to the same basin in parameter space, and then we merge them for our final results. The phase-space density of points in the chain is an estimate of the joint *a posteriori* probability distribution of all the parameters, from which may be calculated the probability distribution for an individual parameter by marginalizing over all of the others.

The fitting procedure had 4 basic steps. First, we performed a joint fit of all the light curves along with the radial velocities, to determine provisional values of the orbital period and physical parameters. Second, we measured individual midtransit times, by performing a MCMC analysis of each light curve with only three free parameters: the zero point and slope of the linear function describing the out-of-transit flux, and the midtransit time. We fixed R_p , R_* , and i at the best-fitting values determined from the ensemble. There is no need to fit the midtransit times simultaneously with $\{R_p, R_*, i\}$ because the errors in those parameters are uncorrelated with the error in the midtransit time. Third, we recomputed the transit ephemeris using the newly measured midtransit times (see § 4.2 for more details

on this step). Fourth, we fixed the orbital period and midtransit times at the values just determined, and performed another joint fit of all the radial-velocity and photometric data, to obtain final estimates of the model parameters and their uncertainties. The results from this final computation did not differ significantly from the results of the initial joint fit.

As mentioned previously, we used two different methods to estimate the factor β by which time-correlated noise effectively increases the flux uncertainties. We refer to the first method as the “time-averaging” method, which has been described previously by Winn et al. (2007b) and is closely related to a method used by Gillon et al. (2006). For each light curve we found the best-fitting model and calculated σ_1 , the standard deviation of the unbinned residuals between the observed and calculated fluxes. Next we averaged the residuals into M bins of N points and calculated the standard deviation σ_N of the binned residuals. In the absence of red noise, we would have expected¹

$$\sigma_N = \frac{\sigma_1}{\sqrt{N}} \sqrt{\frac{M}{M-1}}, \quad (2)$$

but often σ_N is larger than this by a factor β . We found that β depends only weakly on the choice of averaging time τ , generally rising to an asymptotic value at $\tau \approx 10$ min. We denote by β_1 the median of these factors when using averaging times ranging from 15-30 min (the approximate duration of ingress or egress).

We refer to the second method as the “rosary-bead” method, which has been used previously by many investigators (e.g., Bouchy et al. 2005, Southworth 2008). For each light curve, we found the best-fitting model and computed the time series of N residuals. We then added these residuals to the model light curve after time-shifting them by M samples with a periodic boundary condition, i.e., the i th residual was assigned to the time stamp $(i + M) \bmod N$. We repeated this for all $M < N$, then fitted each of these synthetic light curves and took the standard deviation of the results to be the error estimates for the parameters. This is a variant of the well-known bootstrap technique that preserves the temporal correlations among the residuals. We denote by β_2 the ratio between the error estimate returned by the rosary-bead method, and the error estimate assuming uncorrelated errors.

In general β_1 and β_2 are specific to each parameter of the model, but for simplicity we assumed they are the same for all parameters, and to calculate them we focused on the determination of midtransit times. For each of the 13 light curves we compared the error bar

¹We thank G. Kovacs for pointing out that we erroneously neglected the factor $\sqrt{M/(M-1)}$ in previous analyses. Typically $M > 5$ and this factor is smaller than 1.12.

in T_c as obtained through the time-averaging method, and as obtained with the rosary-bead method. For the 13 light curves, β_2/β_1 varied from 0.86 to 1.47, with a mean of 1.13 and a standard deviation of 0.21. Thus the two methods gave similar results, and the rosary-bead method tended to produce larger error estimates. For our final results, we assigned each light curve the value $\beta = \max(\beta_1, \beta_2)$. These choices of β are given in Table 1. All of these procedures may be fairly criticized for lacking statistical rigor, but experience has shown that the more common procedure of setting $\sigma_{f,i} = \sigma_1$ results in underestimated uncertainties in the model parameters, as demonstrated by a lack of agreement between the results of different but presumably equivalent data sets.

4. Results

Table 1 gives all of the newly measured transit times. Table 3 gives the results for the planetary, stellar, and orbital parameters, as well as many other quantities of intrinsic interest or importance for planning follow-up observations. As an example of the latter, the quantity $(R_p/a)^2$ is the planet-to-star flux ratio at opposition, for a geometric albedo of unity, and as such it is relevant to pursuing observations of reflected light from the planet. Another example is the amplitude of the Rossiter-McLaughlin effect, given by $(R_p/R_\star)^2(v \sin i_\star)$, where $v \sin i_\star$ is the projected rotation rate of the star (see, e.g., Gaudi & Winn 2007). The labels A–E, explained in the table caption, are an attempt to clarify which quantities are determined independently from our analysis, which quantities are functions of those independent parameters, and which quantities depend on our isochrone analysis to break the fitting degeneracy between the stellar mass and radius. Table 4 gives the results for the limb-darkening coefficients.

4.1. The stellar and planetary radii

As discussed in the previous section, the joint analysis of the light curves and velocities cannot independently determine the masses and radii of both bodies. Some external information about the star or the planet must be introduced to break the fitting degeneracies $M_p \propto M_\star^{2/3}$ and $R_p \propto R_\star \propto M_\star^{1/3}$. Our approach was to seek consistency between the observed spectroscopic properties of the star, the stellar mean density that is derived from the transit light curves, and theoretical models of stellar evolution. This is the same approach (and uses the same software) that was described in detail by Sozzetti et al. (2007) and Torres et al. (2008). Here we summarize the procedure, and refer the reader to those papers for more details.

There were two sets of inputs. First, we used the values of the effective temperature T_{eff} , surface gravity $\log g$, and metallicity $[\text{Fe}/\text{H}]$ of the host star, as reported by JK, based on a parametric fit to the optical spectrum of XO-3 using the *Spectroscopy Made Easy* (SME) program (Valenti & Piskunov 1996, Valenti & Fischer 2005). Second, we used the scaled semimajor axis a/R_{\star} and the orbital parameters from our joint analysis of the photometry and radial-velocity data. Given a/R_{\star} and the orbital parameters, it is possible to derive the mean stellar density, using Kepler’s Law (Seager & Mallen-Ornelas 2003). We use the symbol ρ_{\star} to refer to the mean density determined in this fashion.

We used the Yonsei-Yale (Y^2) stellar evolution models by Yi et al. (2001) and Demarque et al. (2004). We computed isochrones for the full range of metallicities allowed by the data, and for stellar ages ranging from 0.1 to 14 Gyr, seeking points that gave agreement with the observed T_{eff} and one of the two gravity indicators ($\log g$ and ρ_{\star}). For each stellar property (mass, radius, and age), we took a weighted average of the points on each isochrone. The weights were based on the agreement with the observed temperature, metallicity, and gravity indicator, and a factor taking into account the number density of stars along each isochrone (assuming a Salpeter mass function).

In almost all of the 23 cases examined by Torres et al. (2008), the results when using either $\log g$ or ρ_{\star} as the gravity indicator were in agreement, and greater precision was obtained with ρ_{\star} , often by a factor of 2 or more. Torres et al. (2008) did not consider the case of XO-3, but using the same technique we find poor agreement between the results of using the two independent gravity indicators. Using ρ_{\star} results in a less massive and smaller star, with a higher mean density and a stronger surface gravity. This in turn gives a less massive and smaller planet. One way to frame the discrepancy is that by using ρ_{\star} as the gravity indicator, the isochrone analysis gives a stellar surface gravity of $(\log g)_{\text{phot}} = 4.244 \pm 0.041$, as compared to the SME-derived value of $\log g = 3.950 \pm 0.062$. The difference is 0.294 ± 0.074 , which is inconsistent with zero at the 4σ level. Clearly something is amiss with either our interpretation of the light curve, or the SME determination of $\log g$, or both. The same conflict was already apparent between the light-curve analysis and the isochrone analysis of JK. We have improved the precision of the light-curve parameters by factors of 3 or more, and the conflict with the spectroscopic determination of $\log g$ has been sharpened.

Some further thoughts on the tension between ρ_{\star} and $\log g$ are given in § 5. For the results given in Table 3, we proceeded under the assumption that the error in the spectroscopic determination of $\log g$ was greatly underestimated. We disregarded the spectroscopic $\log g$ while performing the isochrone analysis, and we also increased the error bars on T_{eff} and $[\text{Fe}/\text{H}]$, since the errors in those three quantities are highly correlated when fitting models to the features observed in optical spectra. We increased the error in T_{eff} from 50 K to 100 K,

and in [Fe/H] from 0.023 dex to 0.08 dex, which we believe to be conservative choices, and are consistent with similar judgments made by Torres et al. (2008) in their homogeneous analysis of transiting systems.

4.2. The transit and occultation ephemerides

We calculated a photometric ephemeris for the transits of XO-3 using the 13 midtransit times given in Table 1 and the 16 midtransit times measured by the XO Extended Team and reported previously by JK. We fitted a linear function of transit epoch E ,

$$T_c(E) = T_c(0) + EP. \quad (3)$$

The fit had $\chi^2 = 29.6$ with 27 degrees of freedom, or $\chi^2/N_{\text{dof}} = 1.10$. The results were $T_c(0) = 2454449.86816 \pm 0.00023$ [HJD] and $P = 3.1915239 \pm 0.0000068$ days. Our derived period agrees with the value 3.19154 ± 0.00014 days determined by JK and is about 20 times more precise. Figure 4 is the O–C (observed minus calculated) diagram for the transit times. In this calculation, we did not use the 4 midtransit times that were based on data from the XO survey instrument, because those data had unquantified and apparently large uncertainties. Nevertheless, all of the observed times are plotted in Figure 3, and are seen to be at least roughly consistent with the new ephemeris.

To help in planning observations of occultations (secondary eclipses) of XO-3b, we have also used our model results to predict the timing, duration, and impact parameter of the occultations. Because of the eccentric orbit, occultations and transits are not separated by exactly one-half of the orbital period, and do not have the same duration or impact parameter. Based on our model of the system, we expect occultations to occur 2.109 ± 0.034 days after transits. The predicted occultation ephemeris is given in Table 3.

5. Summary and Discussion

We have presented new photometry spanning transits of the exoplanet XO-3. The photometry greatly improves the precision with which the light-curve parameters are known. In particular, the planet-to-star radius ratio is known to within 0.6%, an improvement by a factor of 6. The inclination angle is now known to within 0.54 deg, an improvement by a factor of 2.5. A third light-curve parameter, the scaled semimajor axis (a/R_\star), has also been refined by a factor of a few, and was used (along with the orbital period and Kepler’s Law) to calculate ρ_\star , the stellar mean density. We found that the photometric result for ρ_\star is incompatible (at the 4σ level) with the previous spectroscopic determination of $\log g$, in

the sense that theoretical stellar-evolution models cannot accommodate both values along with the observed effective temperature and metallicity of the star.

Because of this conflict, it is worth reviewing how ρ_* and $\log g$ were determined. The photometric determination of ρ_* is based on a fit to the light curve with 3 relevant free parameters, and the application of Kepler’s Law (Seager & Mallen-Ornelas 2003). The spectroscopic determination of $\log g$ is based on the interpretation of pressure-sensitive features of the stellar spectrum, especially the widths of the wings of selected absorption lines. The interpretation is performed by comparison to theoretical models of stellar atmospheres. For XO-3 this comparison was performed with SME (Valenti & Piskunov 1996, Valenti & Fischer 2005), an automated analysis program that fits a model to an optical spectrum by adjusting many free parameters, of which the most relevant are the effective temperature, surface gravity, projected rotation rate, and metal abundances. The model is based on plane-parallel stellar atmosphere models in local thermodynamic equilibrium, and reasonable assumptions regarding instrumental broadening and turbulent broadening mechanisms. Empirical corrections are applied to the parameters based on an SME analysis of the Solar spectrum.

The spectroscopic method for determining $\log g$ is more complex than the photometric method for determining ρ_* . In addition, it is important to recognize that the quoted error in the spectroscopic determination of JK ($\log g = 3.950 \pm 0.062$) represents the standard error of the mean of the results of fitting 10 independent spectra of XO-3. Thus, the error bar refers to the repeatability or precision of the result, and not its accuracy. Valenti & Fischer (2005) assessed the accuracy of SME by comparing two methods of determining surface gravity: (1) the purely spectroscopic method described in the previous paragraph; (2) the surface gravity that follows from the observed stellar luminosity (for stars with measured parallaxes), effective temperature, and metallicity, by requiring consistency with theoretical isochrones of stellar-evolution models. They found a systematic offset of 0.1 dex and a large scatter (see § 7.4 of that work). JK repeated this comparison for stars with similar temperatures to XO-3, finding a scatter of about 0.1 dex and some cases in which the discrepancy is ≈ 0.3 dex. Valenti & Fischer (2005) also compared the SME results for $\log g$ with spectroscopic results that have been obtained by other authors, finding a scatter of about 0.15 dex, and discrepancies as large as 0.3 dex. These general comparisons cannot speak to the specific case of XO-3, but they suggest that the 4σ discrepancy between the spectroscopic and photometric methods in the present study is not as serious as it may seem. The true error in the spectroscopic determination of $\log g$ is probably larger than 0.062.

An upward revision of the stellar $\log g$ corresponds to a downward revision of the planetary radius, to $1.217 \pm 0.073 R_{\text{Jup}}$. How does this result compare to the radius that is expected

on theoretical grounds? Fortney et al. (2007) have computed models for planets over a wide range of masses, compositions, ages, and irradiation levels, and provided the results in a convenient tabular form. Interpolation of those tables for a coreless, pure hydrogen-helium planet with properties appropriate for the XO-3 system ($M_p = 11.8 M_{\text{Jup}}$, $a = 0.045$ AU, $L_\star = 2.9 L_\odot$, age 2.82 Gyr) gives a theoretical radius of $1.14 R_{\text{Jup}}$.

Adding as much as $\sim 100 M_\oplus$ of heavy elements would decrease the theoretical radius by a few per cent. On the other hand, the models of Fortney et al. (2008) define the planetary surface as the 1 bar pressure level, whereas a much lower pressure is appropriate for comparison to transit observations. This “transit radius effect” will increase the theoretical radius by a few per cent (Burrows et al. 2007). Assuming the combination of these effects to be small, the observed radius is 1σ larger than the theoretical radius. Thus, the photometric analysis leads to a planetary radius that is only a little larger than the models of Fortney et al. (2007) would predict, similar to the case of HAT-P-1b (Winn et al. 2007b), and not nearly as “inflated” as some other examples in the literature such as HD 209458b (Charbonneau et al. 2000, Henry et al. 2000), WASP-1b (Collier Cameron et al. 2007, Charbonneau et al. 2007b), and TrES-4b (Mandushev et al. 2007).

Although we have argued that the photometric determination of ρ_\star should take precedence over the spectroscopic determination of $\log g$, it would be more definitive to settle the issue by measuring the trigonometric parallax of XO-3, as suggested by JK. Our photometric analysis predicts that the distance will be found to be 174 ± 18 pc, based on the stellar luminosity inferred from theoretical isochrones, the V magnitude of 9.80 ± 0.03 , and the assumption of negligible extinction. The spectroscopic analysis of JK predicted a greater distance, 260 ± 23 pc. An interesting but more challenging prospect for determining the stellar mass (and hence its radius) is to measure the general-relativistic periastron precession of $2'$ yr^{-1} by precise long-term timing of transits and occultations (Heyl & Gladman 2007).

In addition to pinning down the correct value of the radius, there are other reasons to pursue further observations of XO-3, of which many are related to its sizable orbital eccentricity. One consequence of the eccentricity is that the planet experiences significant variations in stellar insolation over the 3.2 d orbital period. The time-variable response of the planet’s atmosphere may be detectable through mid-infrared photometry (Langton & Laughlin 2008). Whatever mechanism produced the large eccentricity may also have produced a large inclination angle relative to the stellar equatorial plane, an angle that can be measured through observations of the Rossiter-McLaughlin effect. Narita et al. (2007) have presented this type of evidence for a significant orbital tilt in the HD 17156 system.

If, on the other hand, the stellar rotation axis is well-aligned with the orbital axis, then the combination of the measurements of $v \sin i$, i , and R_\star give a stellar rotation period of

$P_{\text{rot}} = 3.73 \pm 0.23$ days. This is not too far from the orbital period of 3.19 days, suggesting that spin-orbit interactions may be unusually strong, perhaps even strong enough to excite the orbital eccentricity to the observed value.

Another way to produce an eccentricity is through stable long-term gravitational interactions with another planet. Although the midtransit times we have recorded are nearly consistent with a constant period, and hence do not provide *prima facie* evidence for any additional bodies in the system, we have achieved a precision of 1-2 min using relatively small telescopes. After a few more seasons, a pattern may yet emerge.

We thank the anonymous referee for several insightful suggestions. We are grateful for partial support for this work from NASA Origins grants NNG06GH69G (to M.J.H.), NNG04LG89G (to G.T.), 05-SSO05-86 (to C.M.J.-K.), and NAG5-13130 (to P.R.M.). This work was also partly supported by Grant no. 2006234 from the United States–Israel Binational Science Foundation (BSF), Jerusalem, Israel. KeplerCam was developed with partial support from the Kepler Mission under NASA Cooperative Agreement NCC2-1390 and the KeplerCam observations described in this paper were partly supported by grants from the Kepler Mission to SAO and PSI.

REFERENCES

- Agol, E., Steffen, J., Sari, R., & Clarkson, W. 2005, MNRAS, 359, 567
- Bakos, G. Á., et al. 2007, ApJ, 656, 552
- Bodenheimer, P., Laughlin, G., & Lin, D. N. C. 2003, ApJ, 592, 555
- Bouchy, F., Pont, F., Melo, C., Santos, N. C., Mayor, M., Queloz, D., & Udry, S. 2005, A&A, 431, 1105
- Brosch, N., Polishook, D., Shporer, A., Kaspi, S., Berwald, A., & Manulis, I. 2008, ArXiv e-prints, 802, arXiv:0802.0821
- Burke, C. J., et al. 2007, ApJ, 671, 2115
- Burrows, A., Hubeny, I., Budaj, J., & Hubbard, W. B. 2007, ApJ, 661, 502
- Cameron, A. C., et al. 2007, MNRAS, 375, 951
- Chabrier, G., & Baraffe, I. 2007, ApJ, 661, L81

- Charbonneau, D., Brown, T. M., Latham, D. W., & Mayor, M. 2000, *ApJ*, 529, L45
- Charbonneau, D., Brown, T. M., Burrows, A., & Laughlin, G. 2007a, *Protostars and Planets V*, 701
- Charbonneau, D., Winn, J. N., Everett, M. E., Latham, D. W., Holman, M. J., Esquerdo, G. A., & O'Donovan, F. T. 2007b, *ApJ*, 658, 1322
- Claret, A. 2000, *A&A*, 363, 1081
- Claret 2004, *A&A*, 428, 1001
- Demarque, P., Woo, J.-H., Kim, Y.-C., & Yi, S. K. 2004, *ApJS*, 155, 667
- Ford, E. B. 2005, *AJ*, 129, 1706
- Fortney, J. J., Marley, M. S., & Barnes, J. W. 2007, *ApJ*, 659, 1661
- Gaudi, B. S., & Winn, J. N. 2007, *ApJ*, 655, 550
- Gillon, M., Pont, F., Moutou, C., Bouchy, F., Courbin, F., Sohy, S., & Magain, P. 2006, *A&A*, 459, 24
- Guillot, T., & Showman, A. P. 2002, *A&A*, 385, 156
- Hansen, B. M. S., & Barman, T. 2007, *ApJ*, 671, 861
- Henry, G. W., Marcy, G. W., Butler, R. P., & Vogt, S. S. 2000, *ApJ*, 529, L41
- Heyl, J. S., & Gladman, B. J. 2007, *MNRAS*, 377, 1511
- Holman, M. J., & Murray, N. W. 2005, *Science*, 307, 1288
- Holman, M. J., et al. 2006, *ApJ*, 652, 1715
- Holman, M. J., et al. 2007, *ApJ*, 664, 1185
- Johns-Krull, C. M., et al. 2008, *ArXiv e-prints*, 712, arXiv:0712.4283 [JK]
- Ksanfomality, L. V. 2007, *Solar System Research*, 41, 463
- Langton, J., & Laughlin, G. 2008, *ApJ*, 674, 1106
- Mandel, K., & Agol, E. 2002, *ApJ*, 580, L171
- Mandushev, G., et al. 2007, *ApJ*, 667, L195

- McCullough, P. R., Stys, J. E., Valenti, J. A., Fleming, S. W., Janes, K. A., & Heasley, J. N. 2005, *PASP*, 117, 783
- Narita, N., Sato, B., Ohshima, O., & Winn, J. N. 2007, *ArXiv e-prints*, 712, arXiv:0712.2569
- Seager, S. 2008, *Space Science Reviews*, 11
- Seager, S., & Mallén-Ornelas, G. 2003, *ApJ*, 585, 1038
- Southworth, J., Wheatley, P. J., & Sams, G. 2007, *MNRAS*, 379, L11
- Southworth, J. 2008, *ArXiv e-prints*, 802, arXiv:0802.3764
- Sozzetti, A., Torres, G., Charbonneau, D., Latham, D. W., Holman, M. J., Winn, J. N., Laird, J. B., & O'Donovan, F. T. 2007, *ApJ*, 664, 1190
- Szentgyorgyi, A. H., et al. 2005, *Bulletin of the American Astronomical Society*, 37, 1339
- Tegmark, M., et al. 2004, *Phys. Rev. D*, 69, 103501
- Torres, G., Winn, J. N., & Holman, M. J. 2008, *ArXiv e-prints*, 801, arXiv:0801.1841
- Valenti, J. A., & Piskunov, N. 1996, *A&AS*, 118, 595
- Valenti, J. A., & Fischer, D. A. 2005, *ApJS*, 159, 141
- Winn, J. N., et al. 2007a, *AJ*, 133, 11
- Winn, J. N., et al. 2007b, *AJ*, 134, 1707
- Winn, J. N., et al. 2008, *AJ*, submitted
- Yi, S., Demarque, P., Kim, Y.-C., Lee, Y.-W., Ree, C. H., Lejeune, T., & Barnes, S. 2001, *ApJS*, 136, 417

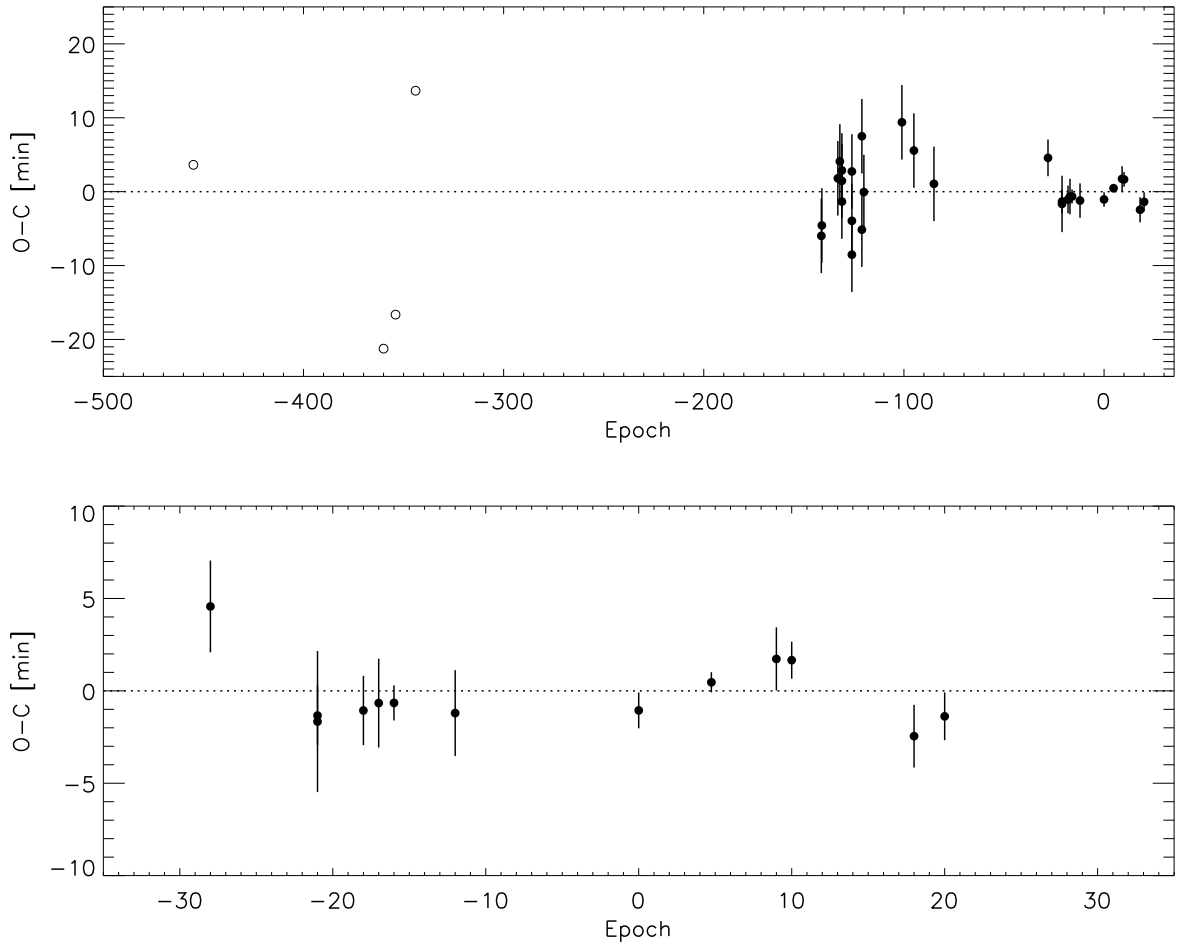


Fig. 4.— Transit timing residuals for XO-3b. The calculated times, using the ephemeris derived in § 4.2, have been subtracted from the observed times. The filled symbols are the data from this work and from the XO Extended Team observations reported by JK. Those data were used to calculate the transit ephemeris. The unfilled symbols are the data from the XO Survey instruments, which were not used to calculate the transit ephemeris.

Table 1. Journal of Observations of XO-3

Date [UT]	Telescope	Filter	Cadence Γ [min ⁻¹]	RMS σ	Red noise factor β	Effective noise $\sigma\beta/\sqrt{\Gamma}$	Midtransit time [HJD]
2007 Sep 16	E. Duran 0.6m	<i>I</i>	0.96	0.0024	2.02	0.0049	2454360.50866 ± 0.00173
2007 Oct 09	V. Cliffs 0.4m	<i>I</i>	0.54	0.0023	3.06	0.0096	2454382.84500 ± 0.00265
2007 Oct 09	V. Cliffs 0.6m	<i>R</i>	1.82	0.0022	1.58	0.0026	2454382.84523 ± 0.00112
2007 Oct 18	E. Duran 0.6m	<i>I</i>	0.96	0.0027	1.18	0.0033	2454392.41999 ± 0.00130
2007 Oct 21	E. Duran 0.6m	<i>I</i>	0.96	0.0022	1.93	0.0043	2454395.61179 ± 0.00167
2007 Oct 24	FLWO 1.2m	<i>z</i>	2.08	0.0023	1.10	0.0017	2454398.80332 ± 0.00066
2007 Nov 06	E. Duran 0.6m	<i>V</i>	0.96	0.0021	1.42	0.0030	2454411.56904 ± 0.00161
2007 Dec 14	FLWO 1.2m	<i>z</i>	2.08	0.0020	1.63	0.0023	2454449.86742 ± 0.00067
2007 Dec 30	FLWO 1.2m	<i>z</i>	2.08	0.0011	1.00	0.0008	2454465.82610 ± 0.00038 ^a
2008 Jan 12	FLWO 1.2m	<i>z</i>	2.50	0.0020	1.31	0.0017	2454478.59308 ± 0.00119 ^a
2008 Jan 15	FLWO 1.2m	<i>z</i>	2.50	0.0018	1.57	0.0018	2454481.78455 ± 0.00070
2008 Feb 10	Wise 0.5m	none	1.61	0.0030	1.18	0.0028	2454507.31319 ± 0.00118
2008 Feb 16	FLWO 1.2m	<i>z</i>	2.50	0.0022	1.69	0.0024	2454513.69768 ± 0.00090

^aOnly a partial transit was observed.

Note. — Column 1 gives the UT date at the start of the night. Column 4 gives Γ , the median number of data points per minute. Column 5 gives σ , the root-mean-squared (RMS) relative flux after subtracting the best-fitting model. Column 6 gives the scaling factor β that was applied to the single-point flux uncertainties to account for red noise (see § 3). Column 7 gives the effective noise per minute, defined as $\sigma\beta/\sqrt{\Gamma}$.

Table 2. Photometry of XO-3

Observatory Code ^a	Filter	Heliocentric Julian Date	Relative flux
1	z	2454398.70513	0.9977
1	z	2454398.70546	1.0000
1	z	2454398.70578	0.9994
1	z	2454398.70611	0.9970
1	z	2454398.70644	0.9975
1	z	2454398.70676	1.0008

^a(1) Fred L. Whipple Observatory 1.2m telescope, Arizona, USA. (2) Wise Observatory 0.5m telescope, Israel. (3) Vermillion Cliffs Observatory 0.4m telescope, Utah, USA. (4) Esteve Duran Observatory 0.6m telescope, Seva, Spain.

Note. — The time stamps represent the Heliocentric Julian Date at the time of mid-exposure. We intend for this Table to appear in entirety in the electronic version of the journal. An excerpt is shown here to illustrate its format. The data are also available from the authors upon request.

Table 3. System Parameters of XO-3

Parameter	Value	68.3% Conf. Limits	Comment
<i>Transit parameters:</i>			
Orbital period, P [d]	3.1915239	± 0.0000068	A
Midtransit time [HJD]	2454449.86816	± 0.00023	A
Planet-to-star radius ratio, R_p/R_\star	0.09057	± 0.00057	A
Orbital inclination, i [deg]	84.20	± 0.54	A
Scaled semimajor axis, a/R_\star	7.07	± 0.31	A
Transit impact parameter	0.705	± 0.023	B
Transit duration [hr]	2.989	± 0.029	B
Transit ingress or egress duration [hr]	0.466	± 0.033	B
RM figure of merit, $(v \sin i_\star)(R_p/R_\star)^2$ [m s $^{-1}$]	152.2	± 2.3	B,C
<i>Occultation parameters (predicted):</i>			
Midoccultation time [HJD]	2454451.977	± 0.034	B
Occultation duration [hr]	2.86	$-0.014, +0.080$	B
Occultation ingress or egress duration [hr]	0.353	$-0.027, +0.067$	B
Occultation impact parameter	0.614	± 0.050	B
Reflected-light figure of merit, $(R_p/a)^2$	0.000164	± 0.000015	B
<i>Other orbital parameters:</i>			
Orbital eccentricity, e	0.260	± 0.017	A
Argument of pericenter, ω [deg]	345.8	± 7.3	A
Velocity semiamplitude, K [m s $^{-1}$]	1463	± 53	A
Planet-to-star mass ratio, M_p/M_\star	0.00927	± 0.00036	E
Semimajor axis [AU]	0.0454	± 0.00082	E
<i>Stellar parameters:</i>			
Mass, M_\star [M_\odot]	1.213	± 0.066	E
Radius, R_\star [R_\odot]	1.377	± 0.083	E
Mean density, ρ_\star [g cm $^{-3}$]	0.650	± 0.086	B
Effective temperature, T_{eff} [K]	6429	± 100	D
Surface gravity, $\log g_\star$ [cgs]	4.244	± 0.041	E
Projected rotation rate, $v \sin i_\star$ [km s $^{-1}$]	18.54	± 0.17	C
Metallicity, [Fe/H]	-0.177	± 0.080	D
Luminosity [L_\odot]	2.92	$-0.48, +0.59$	E
Age [Gyr]	2.82	$-0.82, +0.58$	E
Distance [pc]	174	± 18	E
<i>Planetary parameters:</i>			
M_p [M_{Jup}]	11.79	± 0.59	E
R_p [R_{Jup}]	1.217	± 0.073	E
Surface gravity, $\log g_p$ [cgs]	4.295	± 0.042	B
Mean density, ρ_p [g cm $^{-3}$]	8.1	$-1.3, +1.7$	E
Equilibrium temperature, $T_{\text{eff}}(R_\star/a)^{1/2}$ [K]	1710	± 46	E

Note. — (A) Determined independently from our joint analysis of the photometric and radial-velocity data. (B) Functions of group A parameters. (C) From JK. (D) From JK, with enlarged error bars (see § 4.1). (E) Functions of group A parameters, supplemented by results of the isochrone analysis (see § 4.1) to break the degeneracies $M_p \propto M_\star^{2/3}$, $R_p \propto R_\star \propto M_\star^{1/3}$.

Table 4. Limb-Darkening Parameters for XO-3

Bandpass	Tabulated Values		Fitted Value of
	Linear Coefficient	Quadratic Coefficient	Linear Coefficient
z	0.13	0.35	0.11 ± 0.07
I	0.16	0.36	0.06 ± 0.15
R	0.23	0.37	0.16 ± 0.14
V	0.31	0.36	0.47 ± 0.14
Clear ^a	...	0.33	0.47 ± 0.13

Note. — The assumed limb-darkening law was $I_\mu/I_0 = 1 - a(1 - \mu) - b(1 - \mu)^2$. The tabulated coefficients in Columns 2 and 3 are based on interpolation the ATLAS tables of Claret (2000, 2004), for the stellar parameters $T_{\text{eff}} = 6429$ K, $\log g = 4.244$ (cgs), $[\text{Fe}/\text{H}] = -0.177$ and $v_t = 2.0$ km s⁻¹. Column 4 gives the results of fitting for the linear coefficient when the quadratic coefficient is fixed at the tabulated value.

^aThis entry refers to the (unfiltered) Wise data, for which we used the tabulated quadratic coefficient $b = 0.33$ appropriate for the SDSS g band.